Hindawi
Advances in Materials Science and Engineering
Volume 2023, Article ID 3169912, 15 pages
https://doi.org/10.1155/2023/3169912

Research Article

Experimental Investigation on Shear Strength between Ultra-High-Performance Concrete and Normal Concrete Substrates

Xinghong Jiang,[1,2] **Hengxiang Song**,[3] **Ke Li**,[2] **Jing Qiang**,[4] **and Jing Tian**[5]

[1]*State Key Laboratory of Coal Mine Dynamics and Control, Chongqing University, Chongqing 400044, China*
[2]*China Merchants Chongqing Communications Technology Research Design Institute CO. LTD., Chongqing 4000467, China*
[3]*School of Civil Engineering, Chongqing Jiaotong University, Chongqing 400074, China*
[4]*Hong Kong-Zhuhai-Macao Bridge Authority, Zhuhai 519060, Guangdong, China*
[5]*Key Laboratory of Road and Traffic Engineering of the Ministry of Education, Tongji University, Shanghai 201804, China*

Correspondence should be addressed to Xinghong Jiang; jxh_cq@163.com and Ke Li; 364842342@qq.com

Received 11 July 2022; Revised 13 October 2022; Accepted 17 October 2022; Published 17 February 2023

Academic Editor: Junjie Wang

Tunnel engineering in China has developed to the stage of both construction and maintenance, and the problem of structural defect is widespread. The cast-in-situ jacketed arch treatment takes a long time and has a great impact on traffic. It is urgent to develop prefabricated treatment technology, and the guarantee of mechanical properties of the prefabricated UHPC-post-cast NC interface is the key problem. Through the oblique shear test, combined with the XTDIC full-field strain monitoring system, the failure process and failure mode of UHPC-NC specimens were studied and analyzed under different interface keyway numbers (0, 1, 2, and 3), interface agents (meshless interface agent, cement slurry, silica fume modified cement slurry, modified cement slurry mesh, cement slurry, and expansion agent), and NC pouring grades (*C*30, *C*35, *C*40, and *C*50), as well as the influencing factors of shear strength, shear stiffness, and the slip model of the bonding interface. The results show that there are four typical failure modes in UHPC-NC under compression and shear, including complete interface failure (Class *A*), interface failure + NC shear failure (Class *B*), NC compression failure (Class *C*), and interface failure + NC compression failure + NC slip failure in the keyway (Class *D*). The complete interface failure type (Type *A*) without keyway treatment has sudden failure, and the keyway has the ability to disperse load and limit interface slip. The principal strain decreases along the normal sides of the interface, and the influence range of UHPC and NC sides is about 16.2 mm and 17.5 mm, respectively. In practice, the thinnest part of the treatment structure should not be less than 2 cm. The shear strength of the prefabricated UHPC-post-pouring NC interface is generally low, and the maximum shear strength of 13.9 MPa obtained by the test is still lower than the recommended value of 14–21 MPa of ACI 546.3R-14. In treatment design, the interface shear reinforcement can be introduced to ensure the cooperative bearing capacity. The shear strength of the prefabricated UHPC-post-poured NC interface is slightly affected by the interface agent and postpoured concrete grade and increases linearly with the increase in the number of keyways. When the number of keyways is equivalent to the roughness index, the relationship between the shear strength and the roughness is as follows: $f_s = 1.664 + 3.030R_z$. Under the action of keyway, the interface slip of UHPC-NC can be simplified into four stages: the interface slip stage, the keyway strengthening stage, the shear yield stage, and the specimen failure stage. Based on this, a prefabricated UHPC-post-pouring NC interface slip model was proposed, and the experimental results of key parameters such as interface bond strength, stiffness, and slip amount at different stages were obtained by fitting. In the keyway strengthening stage, the shear stiffness increases linearly first and then tends to be stable with the increase in the number of keyways. The maximum shear stiffness is about 20 MPa/mm, and the maximum interfacial slip increases with the increase in the number of keyways, which improves the overall shear resistance. The results can be used in the design of a tunnel-fabricated treatment segment.

1. Introduction

China has the largest number of and most complex tunnels and underground works in the world, with the fastest speed of development in the future [1]. Citing the 2021 Statistical Bulletin on the Development of the Transportation Industry, as of 2021, the number of highway tunnels in China reached 21,316, with a total length of 21,999.3 km. Among these tunnels, the proportion of long, large tunnels is over 70%, and about 30% of them are in a subhealthy state [2]. China's tunnel works have transitioned from the construction stage to a stage where construction and maintenance are both important [3]. Tunnels are semienclosed underground structures with complex internal and external environments. It is difficult to eliminate their structural defects, and diseases such as cracking and water seepage are widespread. Under the adverse effects of water pressure, freezing and thawing, and fire, disasters such as chip off-falling, water gush, and collapse also occur from time to time [4, 5]. For urban rail transit, high-speed railways, highways, and other lines of communications, the traditional concrete jacketed arch reinforcement method is less applicable as it requires a long operation time and large structural thickness. In combination with the technical development of prefabricated treatment, mechanization, and new materials, the application of new treatment technologies that are fast and efficient with a light structure and no incursion has become a rigid demand and key *R* & *D* orientation for tunnel construction and maintenance [6, 7].

Ultra-high-performance concrete (UHPC) is a new cement-based material with ultra-high strength, ultra-high toughness, and ultra-high durability that is widely used in the treatment and reinforcement of bridges and buildings [8] and has broad application prospects in the prefabricated reinforcement of tunnels [9]. The development of domestic prefabricated treatment technologies is lagging behind, and there is little research on prefabricated treatment technologies combined with new UHPC materials, so the related problems need to be solved. Statistics show that about 50% of reinforcement repair failures are caused by cracking of the bond interface [10]. The interfacial bond reliability of the damaged lining structure (NC) to grouted backfill (NC) to PCL segment (UHPC) is the key to determining the success of reinforcement. PCL is a prefabricated construction method in Japan. The whole process is precast concrete linked.

The interfacial bond strength consists of material bonding strength, mechanical bonding strength, and shear keyway shear strength, which depends on the surface roughness, adhesive, surface cleanliness, and water content. In practical engineering, interfacial cleanliness and wetness are the basic requirements, but the stability of interfacial adhesives is difficult to control and the effect varies [11, 12]. The control of surface roughness is the most critical. Austin et al. [13–16] examined the effect of interface roughness on the bond behavior by using the experimental methods of slant shear, direct shear, pulling, and splitting for ordinary concrete materials. They came up with the interface treatment method of "sandblasting > interface grooving > wire brushing > profile chiseling >> original casting" and proposed the interface roughness calculation method. Tayeh et al. [17], Li and Rangaraju [18], and Feng et al. [19] used postcast UHPC repair as the object and obtained the same conclusions. The investigation shows that for the damaged lining structure (NC) to the grouted backfill (NC) interface, a good effect of collaborative bearing can be achieved by NC sandblasting and chiseling, and the interface properties can be easily guaranteed.

For grouted backfill (NC) to the PCL segment (UHPC) interface, due to the high strength of precast UHPC, the effect of sandblasting and chiseling treatment is significantly reduced, and shear keyway or interface reinforcement is required to improve the interfacial bond strength [20]. Diab et al. [21] and Jafarinejad et al. [22] used cylindrical slant shear tests to derive the mesh grooved treatment. The average 28-day interface shear strengths of the precast and postcast ordinary concrete were 14.4 MPa and 19.5 MPa, respectively, which were 26% and 70% higher than the untreated results. Because of these shear strengths, postcast ordinary concrete mesh groove treatment can greatly improve its shear strengths. Tayeh et al. [17] used prismatic slant shear tests to derive the grid grooved treatment. The 28-day interface shear strength of precast NC-postcast UHPC was 13.63 MPa, 70% higher than the untreated result. Carbonell Munoz et al. [23], Long et al. [24], and Ganesh and Ramachandra Murthy [25] used the same test method with the same grooved form and derived the 28-day shear strengths of the UHPC-NC interface as 17.5 MPa, 20 MPa, and 13.3 MPa. The above investigations show that grooving is beneficial to improving the interface shear capacity, but the improvement is limited and some of the experimental results cannot yet reach the requirement of 14 MPa (interface shear strength) specified by the American Concrete Institute. Mansour and Fayed [26] concluded that the interface shear strengths of UHPC-NC increased by 9–16%, 22–29%, 32–42%, and 41–46% at 3%, 6%, 10%, and 13% of the grooved area, respectively. Increasing the density and scale of the groove and turning the grooves into keyways is another idea to improve the interface shear strength. Xiangguo and Zhang [27] analyzed the effects of shear key and shear angle on the interfacial bond strength and slip displacement of precast UHPC-post-bond NC with direct and slant shear tests. The results show that the interface shear strength is increased by about 20% under single keyway treatment, and the larger the shear angle, the greater the interfacial bond strength and bond stiffness. Yang et al. [28] and Zhang et al. [29] analyzed the interface shear behavior of precast NC-postcast UHPC with different keyway widths, depths, and gaps using direct shear tests. The results show that the interface shear strength is about three times higher than that of the bond treatment after the multiple keyway treatment, and the regular trapezoidal-shaped keyway provides the greatest improvement in the interface shear capacity. In summary, the keyway treatment can significantly improve the interface shear strength and ultimate slip of UHPC-NC, and the degree of improvement is closely related to the number of keyways. Therefore, it can be used as an important orientation for the interface treatment of

prefabricated precast tunnel segments. However, the existing research objects are mainly bridge pier studs or surface courses, through which the interfacial bond behavior of existing NC-postcast UHPC is measured, which is diametrically opposed to the precast UHPC-postcast NC for prefabricated treatment of tunnels in the operation sequence. Although the object of the study by Wu Xiang-guo et al. is prefabricated UHPC, its NC is also prefabricated, which is also different from this study. Due to the dense and smooth characteristics of prefabricated UHPC materials, the interfacial bonding capacity and mechanical bonding capacity are greatly reduced, and the existing findings make it difficult to directly guide the design of prefabricated reinforcement interface treatment of tunnels. The related shear failure strength, slip model, and calculation methods also need further research.

From this, the slant shear test method is used in this article to study the interface shear mechanical properties of precast UHPC-postcast NC under different numbers of interface keyways (0, 1, 2, and 3), while the influence of interface agents (no interface agent, cement slurry, silica fume modified cement slurry, and expansion agent modified cement slurry) and postcast NC grades (*C*30, *C*35, *C*40, and *C*50) on them is considered. The XTDIC system is an optical noncontact three-dimensional deformation measurement system for the measurement and analysis of object surface topology, displacement, and strain. The full-field strain monitoring system (XTDIC) and the universal testing machine are used to observe and analyze the interface failure form, slip process, and shear strength of UHPC-NC. Combining the test results with the design requirements for tunnel reinforcement treatment, the UHPC-NC interface bond shear strength calculation method and the slip model are refined, and the fitting results of relevant parameters are provided based on the experiment.

2. Experimental Plan

2.1. Design of the Experiment. The shear behavior of an interface between precast UHPC and postcast NC is investigated using a slant shear test. The experimental procedures refer to the standard test method for bond strength of epoxy-resin systems used with concrete by slant shear (ASTM C882/C882M-13a). Based on the standard for test methods of concrete physical and mechanical properties (GB/T 50081-2019) and many scholars' findings, the specimen size is taken as 100 mm × 100 mm × 300 mm, and the bond angle is taken as $\alpha = 30^{\circ}$.

This experiment is designed into four working conditions (0, 1, 2, and 4) with the number of interface keyways as the main variable factor of the interface. As for selection of the keyway form, the inward concave keyway form is suitable for this experiment as actual prefabricated treatment of the tunnel is considered, and the outward concave keyway form will obstruct the grouting path and not be conducive to construction. As for selection of the keyway shape, a trapezoidal keyway is used to improve the shear behavior by considering the findings of Zhou Jian-ting and Yang Jun. Dimensions of the specimen and trapezoidal keyway are shown in Figure 1. In addition, two variable factors of the keyway, i.e. the interface agent and strength of postcast concrete, are considered for certain cases. Four levels of each factor are designed as four interface agent treatments (no interface agent, cement slurry, silica fume modified cement slurry, and expansion agent modified cement slurry, respectively), and there are four grades of postcast concrete (*C*30, *C*35, *C*40, and *C*50). For the design of the experiment, K2-NA-40 is the reference group; three specimens are cast for each variable factor, and a total of 30 specimens are fabricated. The main parameters of the specimen are shown in Table 1.

2.2. Specimen Preparation. The specimen production process is as follows:

(1) Experiment preparation: the place-holding wooden block of the same size as NC is made by laser cutting.

(2) UHPC casting: the place-holding wooden block is fixed on one side of the mold as a built-in formwork. The mixed UHPC materials are then poured into the test mold and compacted using an insertion vibrator. The purpose of compaction is to remove air bubbles from the concrete, reduce pores, and make the concrete denser to ensure the quality of the structure. And the flow value of the UHPC mixture used is about 1.8 mm. At the same time, a set of UHPC cubic test blocks is reserved.

(3) UHPC curing: the UHPC specimens are covered with films for curing at room temperature, and the formwork is removed after 24 hours to take out the place-holding wooden block. Wood chips and impurities should be removed from the UHPC interface. After 48-hour steam curing at 90°C high temperature, the specimens are subject to curing at room temperature until the standard age of 7°d.

(4) NC casting: the UHPC is fixed on one side of the mold as a built-in formwork. The mixed NC materials are then poured into the test mold and compacted using an insertion vibrator. At the same time, a set of NC cubic test blocks is reserved.

(5) NC curing: after a 28-day curing period at room temperature, the combined specimens are taken out, and the surface shall be sanded, painted, and sprayed with scattered spots for treatment to complete the production of slant shear specimens.

The specimen production process is shown in Figure 2.

2.3. Material Properties. The experiment is conducted using UHPC produced by a Zhejiang company focused on new types of building materials, whose main raw materials are cement, mineral powder, silica fume, quartz sand, steel fiber, water reducer, and water, and the powder is premixed into bags. The steel fiber is about 10 mm long and 0.12 mm in diameter, with a weight ratio of about 7.1%. And the mix ratio of the UHPC matrix is shown in Table 2.

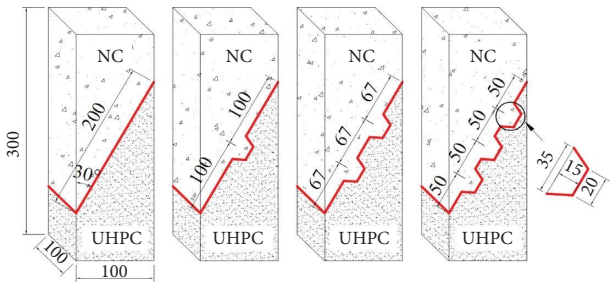

Figure 1: Dimensions of the specimen and trapezoidal keyway of UHPC-NC (unit: mm).

Table 1: Parameters of specimens.

Group	Number of keyways	Bonding materials	Concrete grade	Specimen Qty.
K0-NA-40	0	No interface agent	*C*40	3
K1-NA-40	1			3
K2-NA-40	2			3
K3-NA-40	3			3
K2-CP-40	2	Cement slurry	*C*40	3
K2-SC-40		Silica fume-modified cement slurry		3
K2-EC-40		Expansion agent-modified cement slurry		3
K2-NA-30	2	No interface agent	*C*30	3
K2-NA-35			*C*35	3
K2-NA-50			*C*50	3

Note. (1) Cement slurry is so prepared that the mass ratio of cement to water is 1 : 0.35, and the cement is the P II 52.5 cement. (2) Silica fume-modified cement slurry is so prepared that the mass ratio of cement to silica fume to water is 0.95 : 0.05 : 0.35, and the silica fume is the 970 silica fume. (3) Expansion agent-modified cement slurry is so prepared that the mass ratio of cement to expansion agent to water is 0.9 : 0.1 : 0.35, and the expansion agent is the CSA type expansion agent made in Japan.

Figure 2: The production process of the specimen. (a) Place-holding wooden block cutting. (b) UHPC casting forming. (c) NC casting forming.

Table 2: The mix ratio of the UHPC matrix (unit: kg/m^3).

Component	Cement	Mineral powder	Silica fume	Quartz sand	Steel fiber	Water reducer	Water
Mass	787	244	192	866	157	40	154

The raw materials of *C*30, *C*35, *C*40, and *C*50 concrete include cement, sand, stone, water, and water reducer, and the mix ratio is shown in Table 3.

The reserved test blocks are tested for material properties in accordance with the fundamental characteristics and test methods of ultra-high performance concrete (T/CBMF 37-

Table 3: The mix ratio of normal concrete(kg/m^3).

Strength grade	Cement	Sand	Stone	Water	Water reducer
*C*30	376	704	1148	184	29
*C*35	402	752	1081	165	29
*C*40	415	552	1288	165	29
*C*50	480	638	1185	144	29

2018) and the standard for the test method of mechanical properties on ordinary concrete (GB/T 50081-2002). The cube compressive strength test results of UHPC and NC are shown in Table 4. The 28 d cubic (the specimen size is taken as 100 mm × 100 mm × 100 mm) compressive strength of UHPC obtained from the test is 139.0 MPa. The 28 d cubic (the specimen size is taken as 150 mm × 150 mm × 150 mm) compressive strengths of *C*30, *C*35, *C*40, and *C*50 concrete specimens are 30.6 MPa, 28.6 MPa, 40.9 MPa, and 52.1 MPa, respectively. Due to the insufficient strength of the *C*35 concrete test results, the K2-NA-35 working conditions in the subsequent analysis are not representative, and their relevant results are for reference only.

2.4. Loading and Monitoring Schemes. The electro-hydraulic servo pressure testing machine of Shanghai Hualong Test Instruments Corporation is used for loading. Loading and monitoring devices are shown in Figure 3. During the experiment, the specimen is placed upright on the steel pad of the testing machine. The specimen axis should be adjusted to align with the centers of the upper and lower platens. A force of 5 kN is preloaded for instrument and equipment commissioning. The formal loading speed is controlled at 3 kN/s and loaded to failure. During the loading process, the load and displacement are recorded by the testing machine. The XTDIC of XTOP 3D Technology (Shenzhen) Co., Ltd. is used to monitor the strain of the specimen.

3. Testing Phenomenon and Failure Process

3.1. Failure Mode. During the experiment, there are four main failure modes for the specimen:

(1) Complete interface failure (Class *A*): the specimen is subject to slip failure along the bond interface, and both material interfaces are smooth after slip. No damage and spalling of UHPC and NC were observed on both sides of the interface, and no other forms of cracking of UHPC and NC were observed outside the interface, as shown in Figure 4(a).

(2) Interface failure + NC shear failure (Class *B*): UHPC-NC combined specimens are subject to Class *A* failure at the nonkeyway treated position. There are dense cracks on the NC side at the nonkeyway treated position, with failure eventually penetrating along the direction of the bond interface. Except for a small amount of breakage outside the interface and at the tip of UHPC and NC, the failure is caused by stress concentration based on a preliminary analysis, as shown in Figures 4(b)–4(d).

(3) NC compression failure (Class *C*): during the loading process, the nonkeyway treated position of the interface is subject to Class *A* failure first. As the load increases, the cracks expand vertically along the NC side, and the keyway concrete cracks simultaneously. After the vertical cracks penetrated the interface cracks, the specimen failed. After the failure, a large amount of NC will adhere to the UHPC keyway position.

(4) Interface failure + NC compression failure + NC slip failure in the keyway (Class *D*): a special failure mode emerged during the experiment of K3-NA-40. During the loading process, the condition of the specimen is first consistent with the Class *C* failure. When the upper NC crack penetrated, the NC and UHPC in the upper side shear keyway were detached by tension. As the load increases, it is subject to interface slip failure, as shown in Figure 4(f).

3.2. Failure Process. The full-field principal shear strain monitoring images (by XTDIC) of the specimens with typical failure modes under different ultimate load ratios are shown in Figure 5. The analysis shows that, during the loading process, the red strain failure zone appears at the upper bond interface of the specimen first. With the increase in load, the principal shear strain zone expanded and penetrated along the bond interface, and finally, the specimen failed.

The analysis of the failure mode shows that the upper part of the bond interface failed first during the loading process of the specimens. The main reason is that the difference in material modulus between UHPC and NC causes the load bias, and the stress at the upper part of the bond interface is relatively large during the loading process, so the failure is early. During the loading process, the upper and lower tips are both the failure starting points, which are mainly caused by stress concentration. The end-tangent treatment of the specimen interface has an optimization effect [27].

The analysis of the failure process shows that for specimens without a keyway (Figure 5(a)), the strain failure zone appears early, starting at about 40% of the ultimate load. ,However, the strain diagrams at 60% and 80% limit loads are almost identical to those at 40% limit loads. Before the overall slip of the specimen interface, the strain change is small with a feature of brittle failure. For specimens with keyways (Figures 5(b)–5(f)), as the keyway increases, the contact area of the interface increases, and the shear strain failure zone appears relatively late, starting at about 70% to 80% of the ultimate load. With the increase in load, the

Table 4: Cube compressive strength test results of UHPC and NC (unit: MPa).

Strength grade	28 d compressive strength			Average strength
	Test block 1	Test block 2	Test block 3	
UHPC	130.4	141.1	145.9	139.1
*C*30	31.3	31.0	29.5	30.6
*C*35	35.2	27.7	29.4	28.6
*C*40	40.5	41.2	40.9	40.9
*C*50	52.3	52.9	51.1	52.1

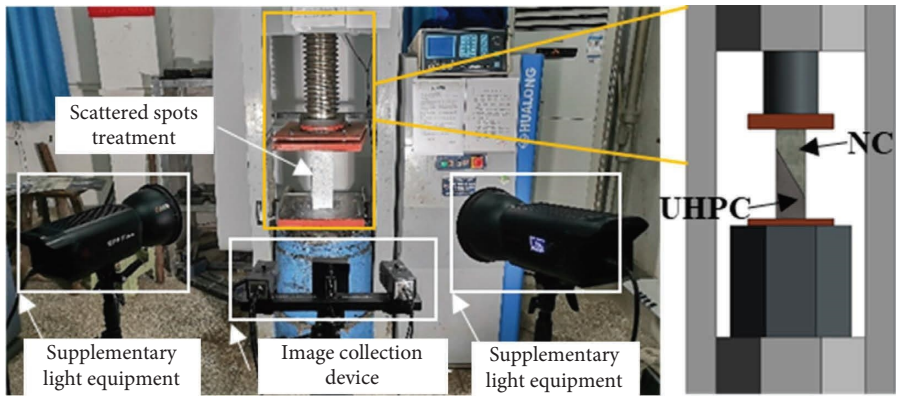

Figure 3: Loading and monitoring devices.

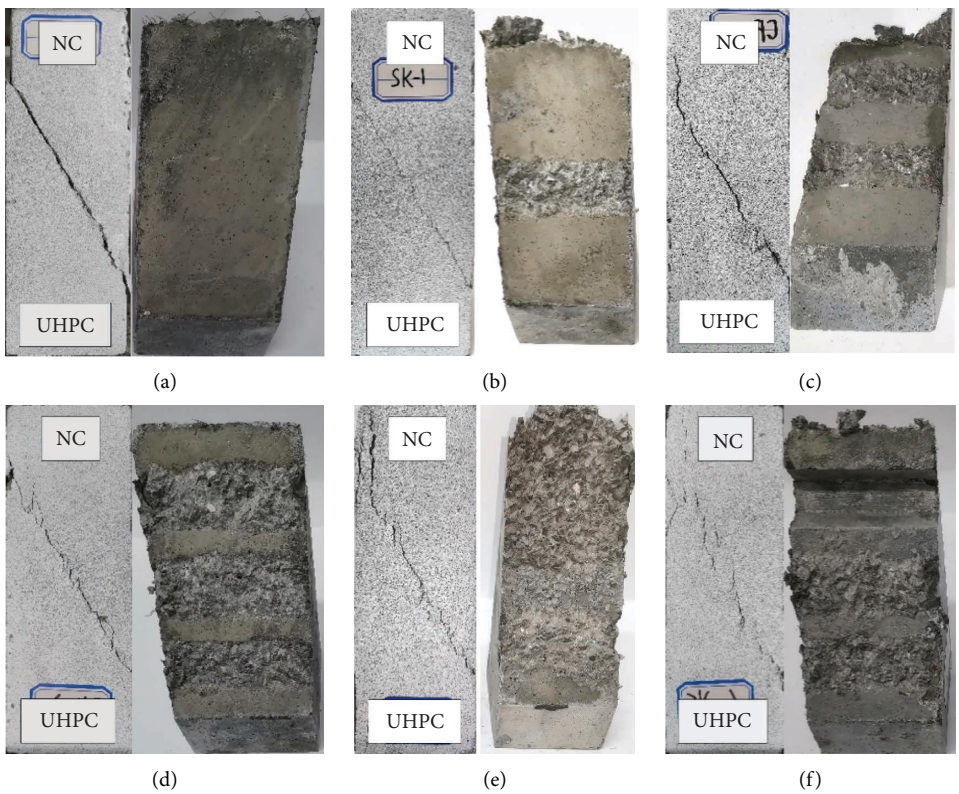

Figure 4: Failure patterns of the specimens. (a) Specimen K0-NA-40. (b) Specimen K1-NA-40. (c) Specimen K2-NA-40. (d) Specimen K3-NA-40-3. (e) Specimen K2-NA-3. (f) Specimen K3-NA-40-1.

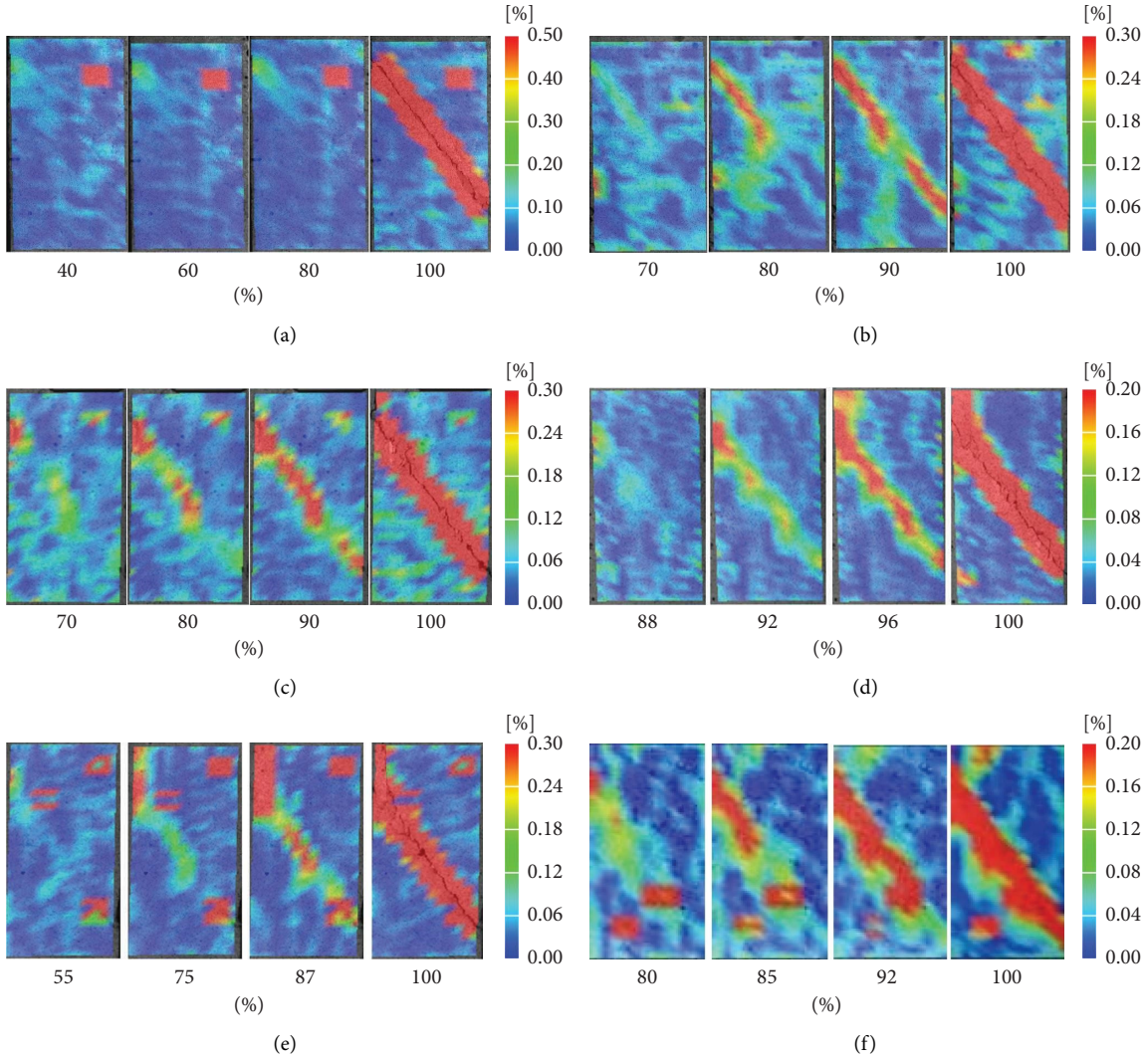

Figure 5: Contour of principal shear strain distribution. (a) Specimen K0-NA-40. (b) Specimen K1-NA-40. (c) Specimen K2-NA-40. (d) Specimen K3-NA-40-3. (e) Specimen K2-NA-30. (f) Specimen K3-NA-40-2.

failure zone gradually expands, and the development process has a certain hysteresis.

Comparing the failure process of the specimens with and without the keyway, it can be seen that without the keyway, with the increase in load, the specimens failed directly through the interface; with the keyway, the principal strain value in the keyway zone is small, and the specimens are first subject to slip failure along the bond interface without a keyway, and then the strain in the keyway zone expands and penetrates until the specimens failed. It can be seen that the presence of the keyway has the ability to limit the interface slip.

3.3. Range of Influence. The strain is measured by a strainometer, and the ultimate load is measured and displayed simultaneously by a universal testing machine. When extracting the ultimate load, strain is also ultimate strain. For the UHPC and NC principal strains along the mid-perpendicular direction of the bond interface, the standard division of $\varepsilon_u = 0.33$ is used to obtain the main range of influence at different numbers of keyways, as shown in Figure 6. From Figure 6(a), it can be seen that the principal strain at the UHPC-NC bond interface of the specimen is the largest under the load and decreases along the normal sides of the interface; the strain at the UHPC side attenuates more rapidly with distance. From Figure 6(b), it can be seen that the range of the influence zone increases under the action of shear keys. When the number of shear keys is 2, the range of the influence zone tends to be stable. Eventually, the major range of influence of UHPC will be about 16.2 mm and about 17.5 mm for the NC side.

4. Result and Analysis

4.1. Analysis of Interface Shear Strength and Influencing Factors

4.1.1. Test Results of Interface Shear Strength. The interfacial bond average strength τ can be calculated from the ratio of

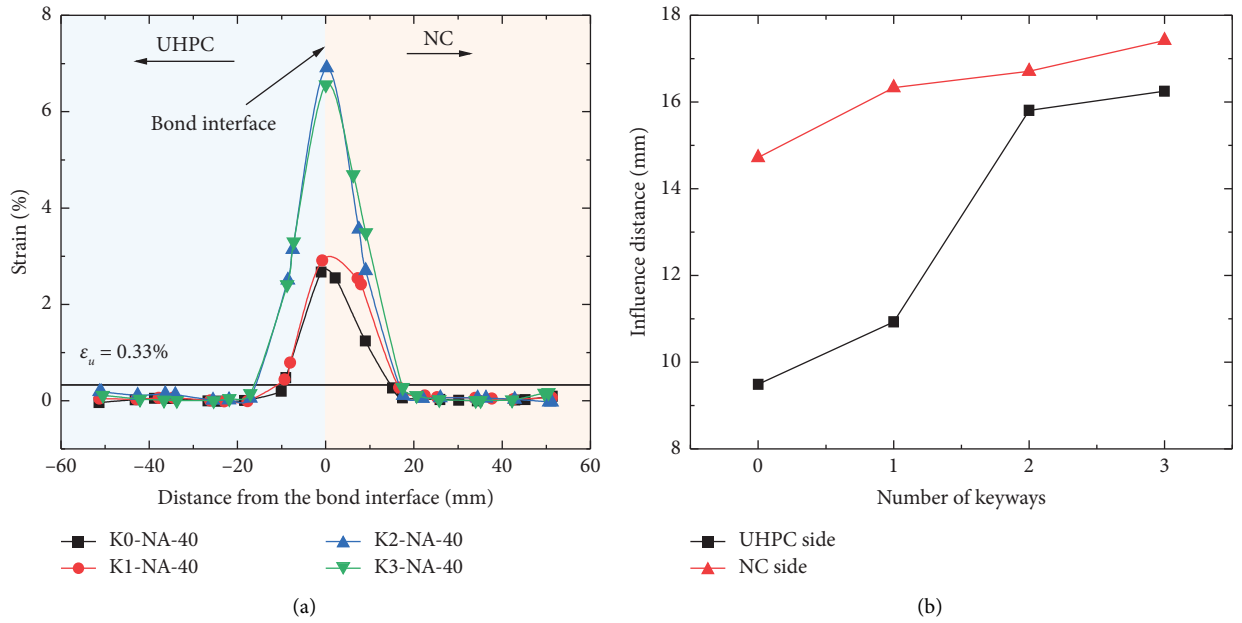

Figure 6: The range of the strain damage zone. (a) Principal shear strain distribution. (b) The range of the influence zone.

the shear force acting on the specimen to the area of the bond interface, $\tau = P\cos^2\alpha/A$, where, P is the axial ultimate load and A is the cross-sectional area of the slant shear specimen. The calculated interface shear bond strength τ, failure mode (M), coefficient of variation (COV), and average shear strength ($\overline{\tau}$) of different specimens are shown in Table 5.

4.1.2. General Status of Interface Shear Strength. Overall, the maximum interface shear strength is the largest (13.9 MPa) when the interface is treated with three keyways and postcast *C*40 concrete. The maximum is smaller than the acceptable range of bond shear strength 14 MPa–21 MPa for the 28 d slant shear test as specified in the guide to materials selection for concrete repair (ACI 546.3R-14); it is also much smaller than the shear strengths of the UHPC-NC interface obtained from the tests conducted by other scholars for the working conditions of precast NC and postcast UHPC, using interface treatments such as grooving and sandblasting (e.g., Table 6). And "the strengths measured in Table 6 has the variation only in the interface treatment." This also shows that the interface shear capacity of the treatment forms of precast UHPC and postcast NC is more unfavorable, and the guarantee of interface properties is more critical to the success of the reinforcement as a whole. In addition to the keyway treatment measures, interface reinforcement can be introduced to ensure good interface mechanical properties.

4.1.3. Analysis of Interface Shear Strength and Influencing Factors. The test results of interface shear strength with different numbers of keyway treatments are shown in Figure 7. It can be seen that the specimen has the weakest shear capacity when no interface keyway is treated, and the maximum shear strength is 2.1 MPa; with the increase in the number of keyways, the interface shear capacity increases linearly. When the number of interface keyways is 3, the maximum shear strength is 13.9 MPa.

Combining the testing failure phenomenon with the analysis of the failure process, it can be seen that the keyway limits the interface slip deformation, improves the interface roughness and friction coefficient, and thus achieves the shear capacity enhancement. Combined with the relevant findings of Pedro on the roughness characteristic index, the average keyway height R_z at the interface is taken as the roughness characteristic index, $R_z = A_J\cos\alpha/A$, where A_J is the width of the specimen multiplied by the waist length of the keyway trapezoid and multiplied by the number of keyways. According to this formula, the roughness indexes of 0, 1, 2, and 3 shear keys are 0, 1.32 mm, 2.645 mm, and 3.97 mm, respectively. The fitted relationship between interface shear strength and roughness is obtained as follows:

$$\begin{aligned} f_s &= 1.664 + 3.030R_z, \\ R^2 &= 0.992. \end{aligned} \tag{1}$$

The shear strengths of the specimens with different postcast concrete strength grades are shown in Figure 8. Since the strength of the cube specimens cured under the same conditions as the *C*35 concrete is approximately equal to the strength of *C*30 and lower than that of *C*35, they can be neglected in the analysis or considered as postcast *C*30 concrete. The analysis shows that there is no trend of increase or decrease in the interface shear capacity with the increase in the grade of the postcast concrete. This is different from Júlio's findings on the interfacial shear behavior for precast NC and postcast UHPC and is also related to the dense properties of UHPC. It also shows that for precast UHPC reinforcement, increasing the interface roughness and providing shear keyways or reinforcement during

Table 5: Interfacial bond shear strength.

Group	Specimen no.	P (kN)	τ (MPa)	M	$\overline{\tau}$ (MPa)
K0-NA-40	K0-NA-40-1	55.1	2.4	A	2.1
	K0-NA-40-2	48.9	2.1	A	
	K0-NA-40-3	34.7	1.5	A	
K1-NA-40	K1-NA-40-1	112.2	4.9	B	5.0
	K1-NA-40-2	124.0	5.4	B	
	K1-NA-40-3	108.7	4.7	B	
K2-NA-40	K2-NA-40-1	209.4	9.1	B	9.7
	K2-NA-40-2	242.0	10.5	B	
	K2-NA-40-3	219.9	9.5	C	
K3-NA-40	K3-NA-40-1	327.6	14.2	D	13.9
	K3-NA-40-2	309.3	13.4	C	
	K3-NA-40-3	326.0	14.1	C	
K2-CP-40	K2-CP-40-1	229.5	9.9	C	9.0
	K2-CP-40-2	207.1	9.0	C	
	K2-CP-40-3	162.8	7.1	B	
K2-SC-40	K2-SC-40-1	206.9	9.0	C	9.0
	K2-SC-40-2	211.8	9.2	C	
	K2-SC-40-3	206.9	9.0	B	
K2-EC-40	K2-EC-40-1	197.9	8.6	B	9.0
	K2-EC-40-2	207.9	9.0	C	
	K2-EC-40-3	215.4	9.3	B	
K2-NA-30	K2-NA-30-1	251.5	10.9	C	10.0
	K2-NA-30-2	158.4	6.9	C	
	K2-NA-30-3	229.9	10.0	C	
K2-NA-35	K2-NA-35-1	262.3	11.4	C	11.4
	K2-NA-35-2	279.2	12.1	B	
	K2-NA-35-3	245.3	10.6	B	
K2-NA-50	K2-NA-50-1	222.7	9.6	B	11.0
	K2-NA-50-2	282.6	12.2	B	
	K2-NA-50-3	253.8	11.0	B	

Note. The test data refer to the standard for the test method of mechanical properties on ordinary concrete (GB/T 50081-2002). Among the three measured values, if the difference between the maximum value or minimum value and the median exceeds 15% of the median, the maximum value and the minimum value are discarded together, and the median is taken as the compressive strength value of the group of specimens. If the difference between the maximum and minimum values and the median exceeds 15% of the median, the test results of the group of specimens are invalid.

Table 6: 30° slant shear strength of other studios.

S/n	Author (s)	Interface treatment	Shear strength (MPa)
1	Xiang-guo and Zhang [27]	Shear key	21.03
2	Robalo et al. [30]	Smooth	13.91
		Steel brush brushing	18.58
		Shallow chiseling	24.64
		Deep chiseling	24.59
3	Tayeh et al. [31]	Sandblasting	14.13
4	Abo Sabah et al. [32]	Grooving	13.63
		Sandblasting	17.74
5	Carbonell Munoz et al. [23]	Grooving	17.5
		Sandblasting	21.7
6	Diab et al. [21]	Wide grooving	14.4
7	Sabah et al. [33]	Grooving	19.4
		Sandblasting	27.0

precast production are more effective treatments than improving the performance of postcast materials.

The shear strength of the specimens with different interface agent treatments is shown in Figure 9. When treating specimens, the shear strength with no interface agent is slightly higher than that of cement slurry, silica fume modified cement slurry, or expansion agent modified cement slurry, but the overall difference is not significant. This

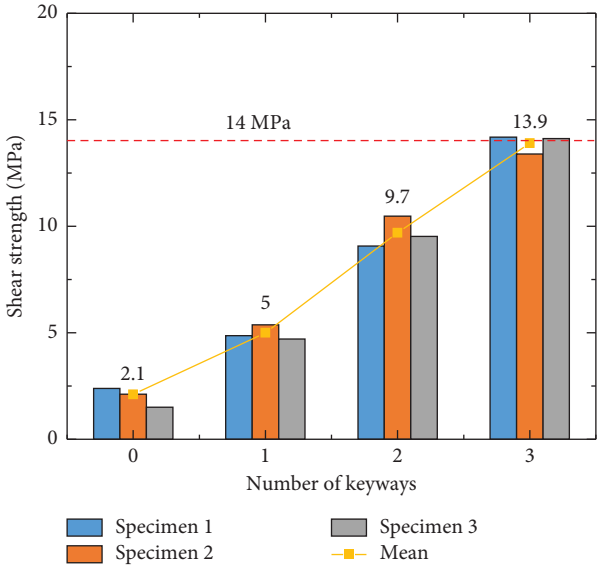

Figure 7: Interfacial bond shear strength with different number of keys.

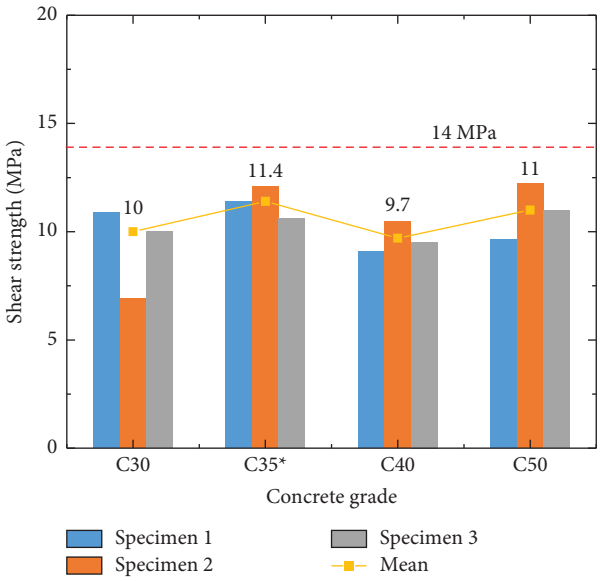

Figure 8: Interfacial bond shear strength with different postcast concrete grades.

shows that for precast UHPC and postcast NC treatment conditions, the interface agents cannot penetrate each other to improve the shear capacity of the interface.

4.2. Analysis of Interface Shear Stiffness and Influencing Factors

4.2.1. Load-Slip Curve. During the experiment, the vertical load and displacement are obtained by the universal testing machine. The interface shear stress and slip are obtained

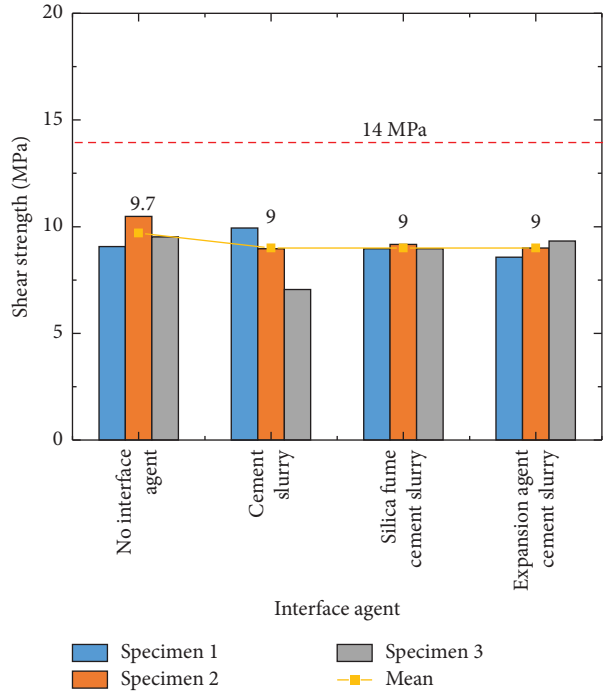

Figure 9: Interfacial bond shear strength with different interfacial agents.

after decomposition (a complete specimen is divided into two parts along the bonding interface) along the bond interface. Slip is measured by a universal pressure testing machine's vertical displacement and then calculated by the Pythagorean theorem along the bond interface. And the shear stress-slip curve relationship is drawn as shown in Figure 10. During the experiment, the data of individual specimens are abnormal and are not indicated in the figure.

4.2.2. Interface Slip Model. Combined with the shear stress-slip curve of the slant shear specimen and the testing phenomenon and failure process, the specimen slip can be divided into four stages: (1) Interface slip stage: the shear capacity at this stage is dominated by the interfacial bonding and mechanical bonding, and the stiffness is relatively small; (2) Keyway strengthening stage: the UHPC-NC interface shear capacity reaches the limit, the keyway concrete plays a role, and the shear stiffness increases and tends to stabilize; (3) Shear yielding stage: the UHPC-NC interface slips, keyway concrete is subject to shear yielding, shear stiffness gradually decreases, and shear strength grows in a nonlinear mode until it reaches its load-carrying limit; (4) Specimen failure stage: the penetrated damage to the keyway concrete causes a rapid decrease in the load-carrying capacity of the specimen and loss of load-carrying capacity. In summary, the shear stages are simplified to a linear process, and the interfacial bond-slip model of precast UHPC and postcast NC is obtained as shown in Figure 11. The expression is as follows:

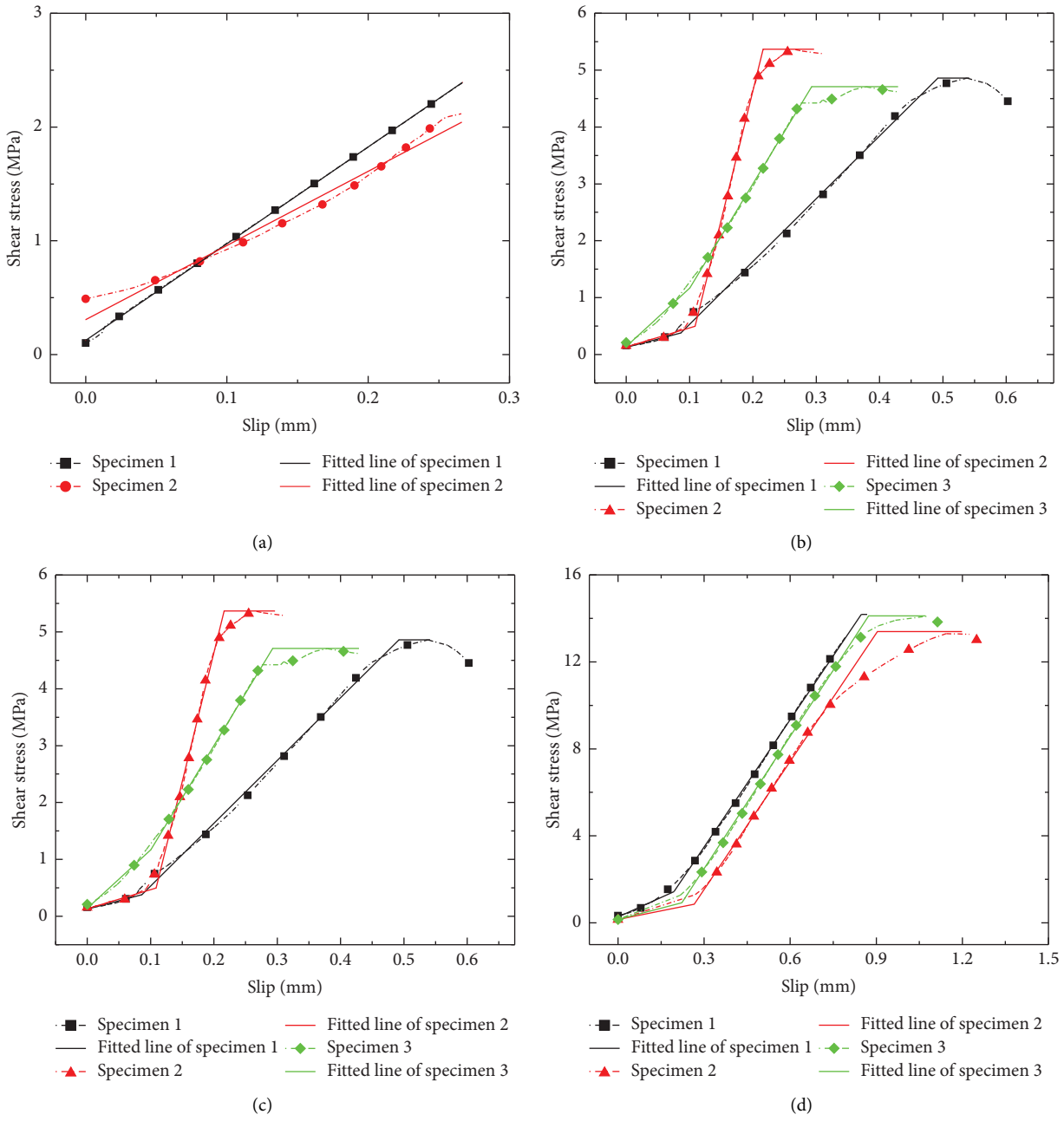

Figure 10: Bond stress-slip of slant shear specimens. (a) No shear keyway. (b) One shear keyway. (c) Two shear keyways. (d) Three shear keyways.

$$\tau = \begin{cases} \overline{K_h} S + \tau_0, & 0 \le S \le S_h, \\ \overline{K_j}(S - S_h) + \tau_h, & S_h < S \le S_q, \\ \tau_u, & S_q < S \le S_u, \\ 0, & S > S_u, \end{cases} \quad (2)$$

where τ is the interfacial bond shear strength (MPa); τ_0 is the bond strength before the interface slip; S_h is the maximum slip at the interface slip stage; τ_h is the maximum shear stress at the interface slip stage; $\overline{K_h}$ is the average shear stiffness at the interface slip stage; τ_u is the ultimate bond strength of the specimen; S_q is the slip when τ_u is reached at the keyway strengthening stage; $\overline{K_j}$ is the average shear stiffness at the keyway strengthening stage; and S_u is the slip when τ_u is reached in the experiment.

The fitting results of the interfacial bond strength, stiffness, and slip with different numbers of keyway treatments are shown in Table 7. The correlation systems of the regression equations are all greater than 0.90, and the regression values have great goodness of fit with the experimental values. Therefore, the model can accurately reflect the interfacial bond-slip mechanical properties of precast UHPC and postcast NC. The second-stage stiffness results obtained from the experiment are similar to the findings of

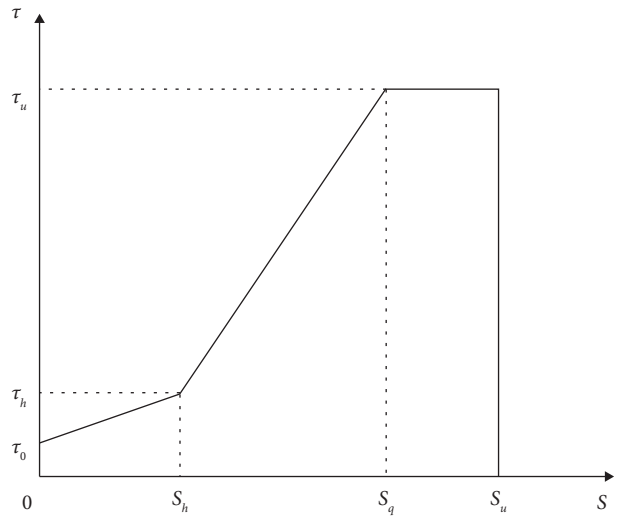

Figure 11: The interfacial bond-slip model.

Table 7: The Interfacial bond strength, bond stiffness, and slip.

Group	Specimen No.	τ_0 (MPa)	S_h (mm)	τ_h (MPa)	$\overline{K_h}$ (MPa/mm)	R_h^2	S_q (mm)	τ_u (MPa)	$\overline{K_j}$ (MPa/mm)	R_j^2	S_u (mm)
K0-NA-40	K0-NA-40-1	0.125	0.267	2.389	8.503	0.999			—		
	K0-NA-40-2	0.308	0.266	2.116	6.516	0.981			—		
K1-NA-40	K1-NA-40-1	0.127	0.086	0.381	2.947	0.924	0.492	4.859	11.028	0.996	0.541
	K1-NA-40-2	0.156	0.109	0.498	3.356	0.953	0.216	5.367	45.297	0.991	0.296
	K1-NA-40-3	0.141	0.100	1.169	10.248	0.975	0.292	4.707	18.393	0.998	0.429
K2-NA-40	K2-NA-40-1	0.161	0.179	1.850	9.411	0.990	0.546	9.065	19.678	0.998	0.621
	K2-NA-40-2	0.144	0.087	1.149	11.447	0.975	0.509	10.478	22.137	0.999	0.713
	K2-NA-40-3	0.137	0.184	0.508	2.014	0.984	0.662	9.520	18.834	0.998	0.726
K3-NA-40	K3-NA-40-1	0.266	0.194	1.435	6.011	0.972	0.848	14.184	19.516	0.999	0.868
	K3-NA-40-2	0.156	0.266	0.855	2.632	0.976	0.903	13.391	19.641	0.998	1.198
	K3-NA-40-3	0.151	0.222	0.920	3.461	0.972	0.873	14.115	20.274	0.998	1.199

Yang et al. [28] on the interfacial bond behavior of UHPC-NC and lower than those of Xiang-guo and Zhang [27]. The main reason concluded from the preliminary analysis is that a larger interfacial shear key was used by Xiang-guo et al.

4.2.3. Interface Slip Influencing Factors. The fitting results of the shear stiffness at the interface slip stage and the keyway strengthening stage with different numbers of keyways are shown in Figure 12. The analysis shows that at the interface slip stage, there is no obvious tendency pattern between the interface shear stiffness and the number of keyways. The main reason is that this stage is the initial stage of loading, and the initial gap and displacement have a large influence on the results. In addition, the critical slip value itself is small at this stage, which is more influenced by other inherent errors. At the keyway strengthening stage, the shear stiffness first increases linearly with the number of keyways and then tends to stabilize with the maximum shear stiffness of about 20 MPa/mm. The main reason is that when the interface roughness reaches a certain level, the interface slip stiffness is mainly influenced by the NC modulus and then tends to stabilize.

The fitting results of the critical slip at the interface slip stage and the keyway strengthening stage with different numbers of keyways are shown in Figure 13. At the interface slip stage, when there is no shear keyway, the slip is large and the specimen is subject to slip failure directly; when the shear keyway exists, the specimen slip is reduced by the shear keyway constraint, and the critical slip grows with the increase in the number of keyways. At the keyway strengthening stage, the maximum slip increases linearly with the increase in the number of keyways, and the continuous improvement of the interfacial ultimate shear capacity is achieved after the stiffness stabilization. The main reason for the formation of this pattern is similar to that for the stabilization of stiffness: because the number of keyways grows, more interface UHPC and NC are involved in the shear process, and the relative slip strain at the interface decreases, realizing the improvement of ultimate strain and shear capacity on the side.

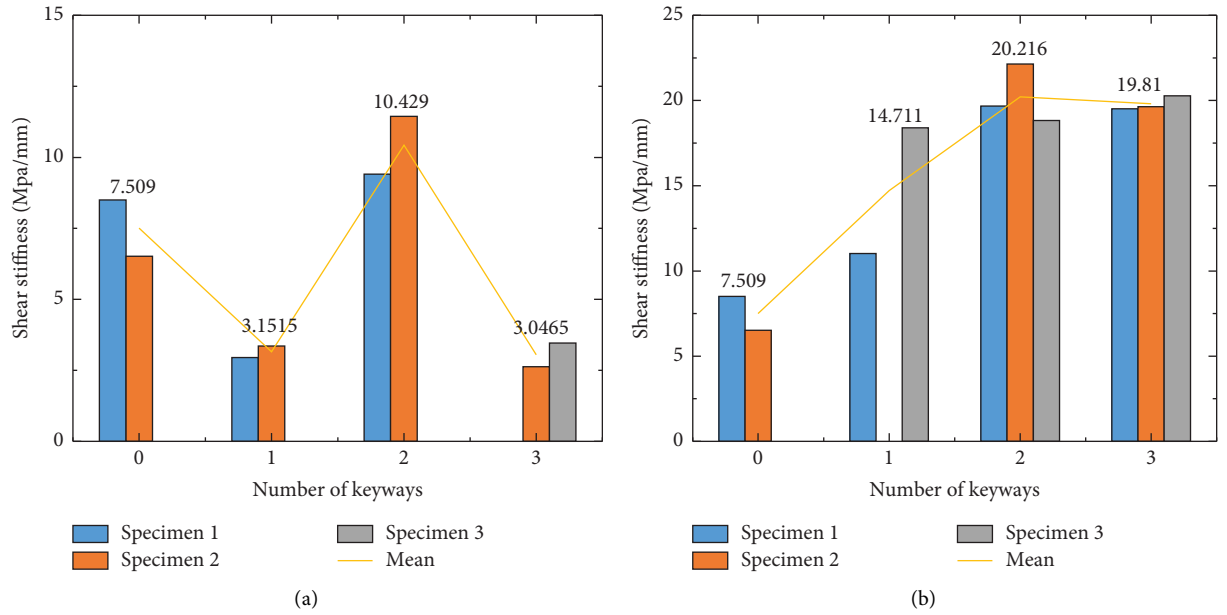

Figure 12: Interfacial bond stiffness with different interfacial agents. (a) The interface slip stage. (b) The keyway strengthening stage.

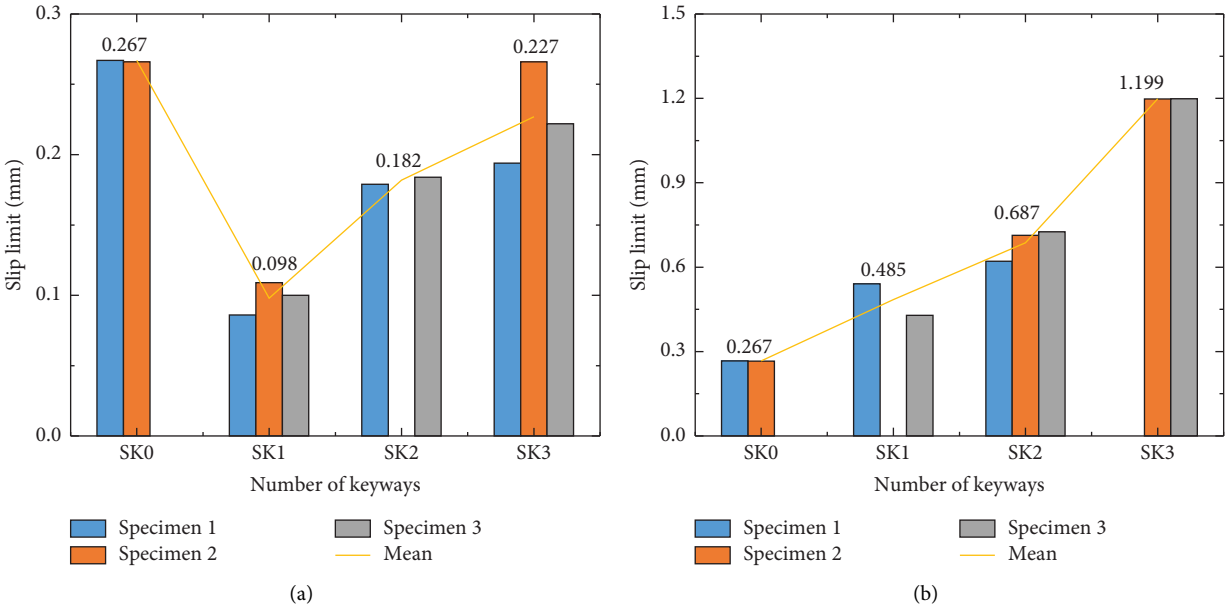

Figure 13: Interfacial slip with different interfacial agents. (a) The interface slip stage. (b) The keyway strengthening stage.

5. Conclusion

This article focuses on the key scientific issues on interfacial bond shear behavior between precast UHPC and postcast NC used in prefabricated treatment of the tunnel, carries out experimental investigation on slant shear strength under working conditions of different numbers of keyways, interface agent treatments, and postcast NC grades, analyzes the failure process and failure mode of UHPC-NC specimens under compression shear, shear strength of bond interface and influencing factors, shear stiffness, and slip model, and draws the following conclusions:

(1) There are four typical failure modes of UHPC-NC under compression shear, namely complete interface failure (Class *A*), interface failure + NC shear failure (Class *B*), NC compression failure (Class *C*), and interface failure + NC compression failure + NC slip failure in the keyway (Class *D*). Class *A* failure is sudden and should be avoided in the works.

(2) The full-field principal strain analysis (by XTDIC) shows that the strain in the keyway zone is much smaller than that in the nonkeyway zone, and the presence of the keyway has the ability to disperse the

load and limit the interface slip. The principal strain decreases along the normal sides of the interface, and the range of influence of UHPC is about 16.2 mm and about 17.5 mm for the NC side. In practice, the thinnest position of the treatment structure should not be lower than 2 cm.

(3) Comparing the findings of this experiment with those of other scholars and specifications, the overall interfacial bond shear strength of precast UHPC-postcast NC is low, and the maximum interface shear strength of 13.9 MPa obtained from the experiment is still smaller than the recommended value of 14–21 MPa specified in ACI 546.3R-14. For the design of prefabricated treatment of the tunnel, interface shear reinforcement can be introduced to ensure collaborative loading.

(4) The interfacial bond shear behavior of precast UHPC-postcast NC is little affected by the interface agent and the grade of postcast concrete and increases linearly with the increase in the number of keyways. Equating the keyway to the interface roughness index R_z, the relationship between interface shear strength and roughness is $f_s = 1.664 + 3.030R_z$. In engineering applications, the interface shear capacity can be improved by increasing the equivalent roughness.

(5) The interface slip of UHPC-NC under the action of the keyway can be simplified into four stages: the interface slip stage, the keyway strengthening stage, the shear yielding stage, and the specimen failure stage. Accordingly, the interface slip model of precast UHPC-postcast NC is proposed, and the findings of key parameters such as interfacial bond strength, stiffness, and slip at different stages are fitted.

(6) At the interface slip stage, there is no tendency pattern between the findings of shear stiffness and the number of keyways due to the initial gap. At the keyway strengthening stage, the shear stiffness first increases linearly with the number of keyways and then tends to stabilize with the maximum shear stiffness of about 20 MPa/mm. The maximum interface slip grows with the number of keyways, resulting in an increase in overall shear capacity.

In this experimental investigation, the findings of interfacial bond mechanical properties of partial precast UHPC-postcast NC are obtained in combination with the slant shear test method, which can be used in the design of the prefabricated tunnel segment. However, some problems were also found in the experiment. For example, the interfacial bond behavior is generally low, so interface shear reinforcement should be provided. The dispersion of stiffness findings at the interface slip stage is large, so further experiments should be conducted. The compression-shear state of UHPC-NC for tunnel reinforcement treatment is complex, so it cannot be fully reflected by this experiment alone. Next, further in-depth investigations will be conducted on these specific problems to realize the implementation of prefabricated tunnel reinforcement treatment technology in China at an early date.

Data Availability

The data supporting the findings of the current study are available from the corresponding author upon request. Requests for access to these data should be made to Jiang Xinghong,641383657@qq.com.

Conflicts of Interest

The authors declare that there are no conflicts of interest.

Acknowledgments

This research was funded by the National Key R&D Program of China (Nos. 2019YFB1600702 and Nos. 2021YFC3002000), the National Natural Science Foundation of China (51978600) and the Chongqing Natural Science Foundation (Distinguished Youth Fund) project(cstc2021jcyj-jqX0012).

References

[1] M. S. Wang, "China has the largest amount of tunnels and underground works in the world with most complicated geological conditions, and has a foreseeable quickest development in the future[J]," *Railway Standard Design*, vol. 1, pp. 1–4, 2003.

[2] H. Ding, Qi Zhang, Y. H. Liu, and F. Chen, "Key problems of tunnel maintenance technology[J]," *China Highway*, vol. 5, pp. 90-91, 2015.

[3] G. Zhongguo, "Editorial department of China journal of highway and transport, review on China's tunnel engineering research:2015[J]," *China Journal of Highway and Transport*, vol. 28, no. 5, pp. 1–65, 2015.

[4] C. Yuan, L. I. Shu-chen, L. I. Shu-cai, and X. Feng, "Study of defects characteristics and repair methods of old tunnel in cold region [J]," *Chinese Journal of Rock Mechanics and Engineering*, vol. 30, no. S1, pp. 3354–3361, 2011.

[5] F. Dong, F. A. N. G. Qian, D. L. Zhang, and L. Shen, "Analysis on defects of operational metro tunnels in beijing[J]," *China Civil Engineering Journal*, vol. 50, no. 6, pp. 104–113, 2017.

[6] H. O. N. G. Kai-rong and F. E. N. G. Huan-huan, "Development trends and views of highway tunnels in China over the past decade," *[J]. China Journal of Highway and Transport*.vol. 33, no. 12, pp. 62–76, 2020.

[7] Si-ming Tan, W. Wang, and G. O. N. G. Jiang-feng, "Development and Prospect of Railway Tunnels in China (including statistics of railway tunnels in China by the end of2020)[J]," *Tunnel Construetion*, vol. 41, no. 2, p. 308, 2021.

[8] S. H. A. O. Xu-dong, W. Fan, and Z.-yu Huang, "Application of ultra-high-performance concrete in engineering structures [J]," *China Civil Engineering Journal*, vol. 54, no. 1, pp. 1–13, 2021.

[9] Editorial Department of China Journal of Highway and Transport, "Review on chinas bridge engineering research: 2021[J]," *China Journal of Highway and Transport*, vol. 34, no. 2, pp. 1–97, 2021.

[10] V. C. Li, "High performance fiber reinforced cementitious composites as durable material for concrete structure repair [J]," *International Journal for Restoration*, vol. 10, no. 2, 2004.

[11] L. A. Modesti, A. S. D. Vargas, and E. L. Schneider, "Repairing concrete with epoxy adhesives," *International Journal of Adhesion and Adhesives*, vol. 101, Article ID 102645, 2020.

[12] N. Sun, Y. Song, W. Hou et al., "Interfacial bond properties between normal strength concrete and epoxy resin concrete," *Advances in Materials Science and Engineering*, vol. 2021, pp. 1–14, Article ID 5561097, 2021.

[13] S. Austin, P. Robins, and Y. Pan, "Shear bond testing of concrete repairs," *Cement and Concrete Research*, vol. 29, no. 7, pp. 1067–1076, 1999.

[14] E. N. B. S. Júlio, F. A. B. Branco, and V. D. Silva, "Concrete-to-concrete bond strength. Influence of the roughness of the substrate surface," *Construction and Building Materials*, vol. 18, no. 9, pp. 675–681, 2004.

[15] E. N. B. S. Júlio, F. A. B. Branco, V. D. Silva, and J. F. Lourenco, "Influence of added concrete compressive strength on adhesion to an existing concrete substrate," *Building and Environment*, vol. 41, no. 12, pp. 1934–1939, 2006.

[16] P. M. D. Santos, E. N. B. S. Júlio, and V. D. Silva, "Correlation between concrete-to-concrete bond strength and the roughness of the substrate surface," *Construction and Building Materials*, vol. 21, no. 8, pp. 1688–1695, 2007.

[17] B. A. Tayeh, B. A. Bakar, M. M. Johari, and M. Ratnam, "The relationship between substrate roughness parameters and bond strength of ultra high-performance fiber concrete," *Journal of Adhesion Science and Technology*, vol. 27, no. 16, pp. 1790–1810, 2013.

[18] Z. Li and P. R. Rangaraju, "Effect of surface roughness on the bond between ultrahigh-performance and precast concrete in bridge deck connections," *Transportation Research Record: Journal of the Transportation Research Board*, vol. 2577, no. 1, pp. 88–96, 2016.

[19] S. Feng, H. Xiao, and J. Geng, "Bond strength between concrete substrate and repair mortar: effect of fibre stiffness and substrate surface roughness," *Cement and Concrete Composites*, vol. 114, Article ID 103746, 2020.

[20] J. T. Zhou, H. U. Tian-xiang, J. Yang, and K. Deng, "Experimental investigation on bonding behavior of UHPC-NC interface in keyway structure[J]," *Materials Reports*, vol. 35, no. 16, pp. 16050–16057, 2021.

[21] A. M. Diab, A. E. M. Abd Elmoaty, and M. R. Tag Eldin, "Slant shear bond strength between self compacting concrete and old concrete," *Construction and Building Materials*, vol. 130, pp. 73–82, 2017.

[22] S. Jafarinejad, A. Rabiee, and M. Shekarchi, "Experimental investigation on the bond strength between Ultra high strength Fiber Reinforced Cementitious Mortar & conventional concrete," *Construction and Building Materials*, vol. 229, Article ID 116814, 2019.

[23] M. A. Carbonell Munoz, D. K. Harris, T. M. Ahlborn, and D. C. Froster, "Bond performance between ultrahigh-performance concrete and normal-strength concrete," *Journal of Materials in Civil Engineering*, vol. 26, no. 8, 2014.

[24] J. Long, Q. Chen, and J. I. A. N. G. Zheng-wu, "Experimental study on the influence of different factors on the bonding strength of UHPC-ordinary concrete[J]," *China Concrete and Cement Products*, vol. 4, pp. 4–8, 2019.

[25] P. Ganesh and A. Ramachandra Murthy, "Simulation of surface preparations to predict the bond behaviour between normal strength concrete and ultra-high performance concrete," *Construction and Building Materials*, vol. 250, Article ID 118871, 2020.

[26] W. Mansour and S. Fayed, "Effect of interfacial surface preparation technique on bond characteristics of both NSC-UHPFRC and NSC-NSC composites," *Structures*, vol. 29, pp. 147–166, 2021.

[27] W. U. Xiang-guo and X.-chen Zhang, "Investigation of short-erm interfacial bond behavior between existing concrete and precast ultra high performance concrete layer[J]," *Journal of Building Structures*, vol. 39, no. 10, pp. 156–163, 2018.

[28] J. Yang, J. T. Zhou, Z. Y. Zhang, and P. Zhano, "Shear performance of keyway interface between UHPC and normal concrete[J]," *China Journal of Highway and Transport*, vol. 34, no. 8, pp. 132–144, 2021.

[29] Y. Zhang, J. Wu, S. H. A. O. Xu-dong, and J. Xiao, "Experiment on interfacial shear properties between ultra high performance concrete and normal strength concrete[J]," *China Civil Engineering Journal*, vol. 54, no. 7, pp. 81–89, 2021.

[30] K. Robalo, R. Do Carmo, H. Costa, and E. Julio, "Experimental study on the interface between low cement recycled aggregates concrete and ultra-high durability concrete," *Construction and Building Materials*, vol. 304, Article ID 124603, 2021.

[31] B. A. Tayeh, B. H. Abu Bakar, and M. A. Megat Johari, "Characterization of the interfacial bond between old concrete substrate and ultra high performance fiber concrete repair composite," *Materials and Structures*, vol. 46, no. 5, pp. 743–753, 2013.

[32] S. H. Abo Sabah, M. H. Hassan, N. Muhamad Bunnori, and M Megat Johari, "Bond strength of the interface between normal concrete substrate and GUSMRC repair material overlay," *Construction and Building Materials*, vol. 216, pp. 261–271, 2019.